One-Port Vector Network Analyzer Characterization of Soil Dielectric Spectrum

Arkadiusz Lewandowski, *Member, IEEE*, Agnieszka Szypłowska, Andrzej Wilczek,
Marcin Kafarski, Justyna Szerement, and Wojciech Skierucha

Abstract—Accurate determination of soil complex-dielectric-permittivity spectrum is important for various applications, especially for the development of soil moisture sensors that can be used, e.g., in agriculture and for environmental monitoring. Wideband measurement of soil dielectric spectrum requires the use of large-diameter coaxial transmission-line cells connected to a vector network analyzer (VNA). We present a new method for soil dielectric-spectrum characterization in the frequency range of 0.05–3 GHz. Our methodology is based on a wideband one-port VNA measurement of a soil sample inserted into a large-diameter coaxial cell. The key part of our approach is the use of a variable load terminating the coaxial cell to extract the scattering parameters of the sample, which are then fed into a dielectric permittivity extraction algorithm. The system provides quick and repeatable measurements without the use of flexible microwave cables. Also, application of a portable one-port VNA significantly lowers the cost of the system in comparison to two-port setups. We verify our methodology based on measurements of reference materials—polytetrafluoroethylene, isopropanol, and ethanol—and then apply it to characterize the soil samples with different moisture content and salinity. Experimental results confirm the validity of our approach.

Index Terms—Calibration, dielectric measurements, microwave measurements, soil measurements, soil moisture and salinity.

I. INTRODUCTION

ACCURATE characterization of soil dielectric properties is important both for fundamental and applied sciences, including agriculture, geosciences, and environmental studies. Measurement of dielectric properties in either the time or frequency domain underlies the operation of many popular soil moisture sensors [1]. In the frequency range of many dielectric soil-moisture sensors, several overlapping dielectric relaxation mechanisms can occur and, consequently, affect the output and accuracy of the sensors [2], [3]. Dielectric relaxation effects in soil may also have an impact on ground penetrating radar (GPR) performance [4]. Also, the knowledge of dielectric properties of soil is necessary for soil-moisture retrieval algorithms in microwave remote sensing [5].

The most common methods used for wideband frequency-domain characterization of material dielectric spectrum are methods based on coaxial open-ended probes and methods employing coaxial or waveguide transmission-line cells [6], [7]. Coaxial open-ended probes that operate in a wide frequency range have, however, limited use for soil measurements due to soil inhomogeneity, thus their performance was positively verified only for fine-grained soils [8]. Consequently, coaxial transmission-line cells have been extensively used for soil dielectric spectrum characterization [9]–[13] due to a larger possible sample volume than in the case of open-ended probes.

All material dielectric-spectrum characterization methods based on a coaxial transmission-line cell use a vector network analyzer (VNA) to measure sample scattering parameters. In order to remove the inevitable systematic errors introduced by the VNA, a full two-port calibration technique is necessary: in the simplest case, this is the short-open-load thru (SOLT) technique [10]–[14]; in a more advanced case, in order to obtain a higher measurement accuracy, a fixed load is replaced by a sliding load [6], [7], or the multiline through–reflect-line (TRL) technique [15] is used [9], [16]. It is important to note that the multiline TRL technique is a benchmark calibration technique with respect to which calibration standards used in all other calibration techniques (such as SOLT) are characterized and verified [17].

In the case of soil or liquid measurement in coaxial transmission-line cells, additional systematic errors are introduced by adapters between the VNA connectors and the large-diameter coaxial transmission line, and the beads supporting the material under test (MUT). The approaches used for characterization of those errors can be divided into approximate and exact ones. Approximate approaches make, in general, some simplifying assumptions. In the simplest case, only the phase shift [11]–[13] or the phase shift and attenuation [10] of the adapters are accounted for while neglecting parasitic mismatches. However, it has been shown that this may lead to significant errors in dielectric spectrum extraction [9]. An attempt to account for parasitic mismatches has been made in [14]. However, it can be easily shown that a simple bilinear model proposed in [14] is applicable only for one-port measurements and cannot represent the complicated behavior

of embedding errors in the two-port case (see [18, eq. (10)] and [19, eqs. (9)–(13)]).

Exact approaches for accounting for the adapters between the VNA connectors and the large-diameter coaxial transmission line are based on VNA calibration performed with calibration standards implemented with the *same* transmission-line type as the one used to hold the MUT sample [6], [7], [9], [16]. Such approaches do not require any assumptions as to the two-port networks describing the adapters between VNA connectors and large-diameter coaxial transmission lines since their scattering parameters are lumped into the VNA calibration coefficients. Moreover, the beads supporting the MUT sample can be separately characterized with full two-port scattering matrices while their impact can be removed based on the transmission matrix approach [9].

Calibrating a VNA with large-diameter coaxial transmission-line ports is a challenging task as there are no standardized connectors suitable for a large number of quick and repeatable connections, nor commercially available calibration standards for such transmission lines. A novel measurement system for soil dielectric spectrum characterization in large-diameter EIA 1 5/8″ coaxial transmission-lines that enables such a calibration was presented in our previous work [9]. This system uses a similar coaxial-transmission line cell as the one described in [10]–[13]; however, instead of using approximate VNA calibration techniques [10]–[13], the multiline TRL calibration method [15] is used. This method—as implemented in [9]—enables accurate VNA measurement directly at arbitrary reference planes inside of the large-diameter coaxial transmission lines. It uses a set of calibration standards implemented with large-diameter coaxial transmission lines: a set of five lines with different lengths and an unknown highly-reflective load realized as a short-circuited transmission-line section (referred to as an offset short). Thus, it enables accurate scattering-matrix measurement of a soil sample inserted into a coaxial cell with the effect of any intermediate devices—such as connectors, adapters and supporting beads—fully corrected for. However, the accuracy of the system presented in [9] is limited, in particular at lower frequencies, due to cable flexure errors. Since the system is based on two-port VNA measurements, cables are necessary to connect the calibration standards and devices under test (DUTs). These cables need to be long enough in order to connect the multiline TRL calibration standards, which in [9] have lengths ranging from 6 to 50 cm. Thus, the system becomes more sensitive to inevitable errors caused by the instability of cable insertion loss and phase shift.

In this paper, we present a new measurement system that has improved repeatability and speed with respect to [9]. The key feature of this system is that it is solely based on one-port VNA measurements and, therefore, the use of cables is avoided. The measurement technique we apply in this new system stems from a well-known adapter characterization and one-port VNA calibration techniques [20]–[23] and is based on a two-step calibration with multiple one-port calibration standards. However, instead of using multiple mechanical standards [20]–[22] or sliding terminations [23], we employ

an electronically switchable termination, referred to as an electronic calibration unit (ECU). By using this unit, we limit the number of mechanical reconnections and, thus, improve the measurement speed and repeatability. We further assume that the ECU reflection coefficients are unknown and determine them along with the one-port VNA calibration coefficients using a new VNA calibration technique. This new technique uses the same set of transmission lines as the multiline TRL method implemented in [9]; however, instead of relying on two-port VNA measurements of the lines, it employs only reflection coefficient measurements of the lines terminated with all of the ECU reflection coefficients. After the system calibration, when the one-port VNA calibration coefficients and the ECU reflection coefficients are known, the input reflection coefficient of the measurement cell terminated with all of the ECU reflection coefficients is measured and from those measurements, scattering parameters of the measurement cell are determined. These parameters, after correcting for the air sections and supporting beads [9] are then fed into a dielectric-spectrum extraction algorithm. Finally, in order to further improve the speed and repeatability of our system, we employ a custom-designed vacuum connection system for EIA 1 5/8″ connectors (patent pending [24]).

II. Measurement System

A photograph of our new system is shown in Fig. 1(a). The key parts of the system are: a one-port VNA (portable VNA R60 from Copper Mountain Technologies with 1–6000 MHz frequency range, and 109-dB dynamic range for 100-Hz IF bandwidth), two Type-N/EIA 1 5/8″ adapters, an EIA 1 5/8″ measurement cell, and an ECU. The ECU was custom-made based on SP4T CMOS switch and four mechanical standards (short, open, matched termination, and offset short implemented as a short adapter terminated with a short circuit), with SMA connectors. The measurements are taken in the frequency range from 50 MHz to 3 GHz.

The measurement cell is shown in Fig. 1(b) and consists of a 60-mm-long coaxial transmission line section of EIA 1 5/8″ standard: the inner diameter of the outer conductor is 38.8 ± 0.075 mm and the outer diameter of the inner conductor is 16.9 ± 0.050 mm [9]. The cell is made out of acid-resistant steel, and two 7.5-mm-thick polyoxymethylene (POM) beads are used to support the MUT. We chose POM due to its very low moisture absorption. The beads are equipped with inner and outer o-rings to prevent water leakage from the cell. The o-rings are made out of nitrile-butadiene rubber which can sustain temperatures from $-40\,°C$ to $+108\,°C$ and is also, unlike natural rubber, resistant to various chemicals.

A custom-designed vacuum connection system [see Fig. 1(b)] is used in order to assure speed and repeatability of connections between the Type-N/EIA 1 5/8″ adapters and the outer conductor of a transmission line [24]. Typically, elements of EIA 1 5/8″ systems are connected using flanges and screws. These screws have to be uniformly tightened in order to provide a repeatable connection between outer conductors, and even a small nonuniformity in the torque may result in a gap between the outer conductors. Thus, the connection procedure
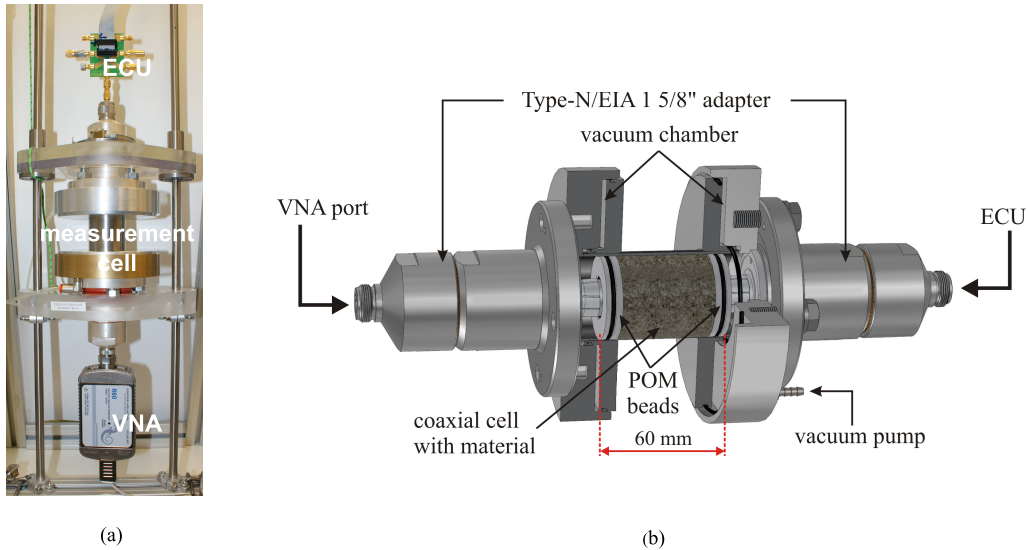
Fig. 1. Measurement system. (a) Photograph and (b) cross section of the measurement cell with the vacuum connectors.

of such flanges is lengthy and prone to operator errors. In our connection system, a vacuum chamber is formed between a customized flange of a Type-N/EIA 1 5/8" adapter and a customized flange of an outer conductor of a transmission line. When the vacuum is created by removing air with a pump, the outer conductors press against each other and make contact. The contact force is determined only by the area of the vacuum chamber elements which improves connection repeatability.

III. MEASUREMENT PROCEDURE

In this section, we discuss the measurement procedure used in our system. We first give an overview of this procedure and then discuss the details of the system calibration, cell scattering-parameters measurement, and dielectric-spectrum extraction.

A. Overview

An overview of the measurement procedure used in our system is shown in Fig. 2. The goal of this procedure is to obtain complex dielectric-permittivity spectrum of the MUT inserted into a coaxial measurement cell [see Fig. 2(c)]. To this end, we start with the system calibration shown in Fig. 2(a). The aim of system calibration is to calculate: 1) one-port VNA calibration coefficients that will allow determining the cell input reflection coefficient Γ from the raw reflection-coefficient measurement $\widetilde{\Gamma}$ and 2) unknown reflection coefficients Γ_m^{ECU}, $m = 1, \ldots, M$ of the electronically switchable termination ECU. These unknown parameters are determined based on the raw reflection coefficient $\widetilde{\Gamma}$ measurements of N transmission lines, each terminated with M unknown reflection coefficients Γ_m^{ECU} (also referred to as the ECU "states"), and of a highly reflective load realized in our system as a short-circuited transmission-line section. Details of this calibration procedure are given in Section III-B.

Once the system is calibrated, we proceed to the measurement of cell scattering parameters [see Fig. 2(b)]. This step
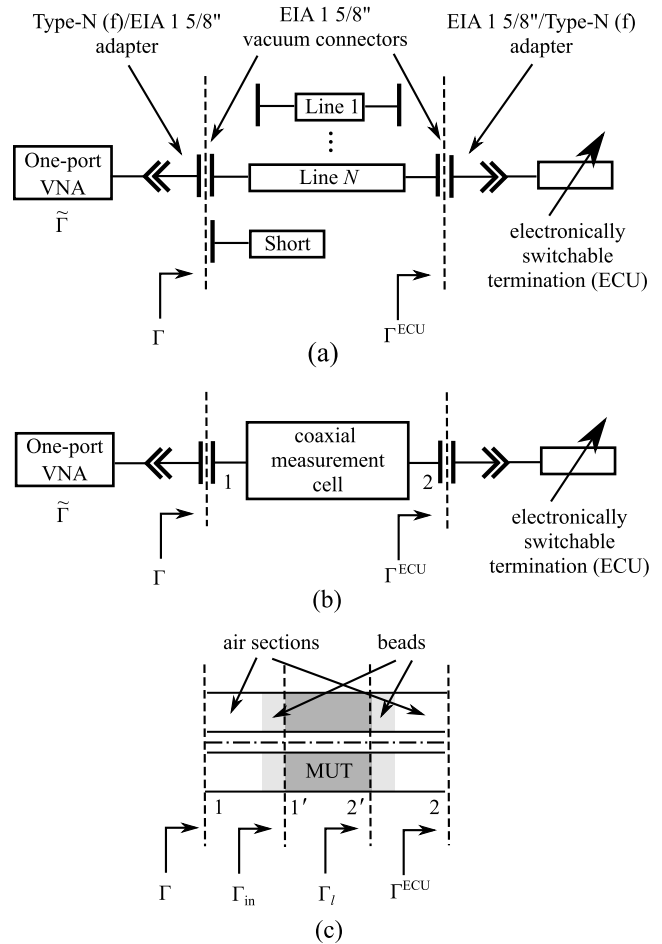

Fig. 2. Measurement procedure overview. (a) System calibration. (b) Measurement of cell scattering parameters. (c) MUT scattering-parameter extraction.

is the *crux* of our method. In a typical transmission/reflection method, cell scattering parameters are measured directly with a calibrated two-port VNA [9]. In our system, these parameters

are determined indirectly by measuring the input reflection coefficient Γ of the cell for a set of different terminations Γ_m^{ECU} realized by the ECU. This is a well-known approach used in microwave measurements for calibrating one-port VNAs and characterizing adapters [20]–[22]. Details of this procedure are described in Section III-C.

Measurement of cell scattering parameters is followed by dielectric spectrum extraction. In the first step of this extraction [see Fig. 2(c)], we calculate MUT scattering parameters (i.e., scattering parameters referenced to planes 1′ and 2′) from cell scattering parameters (referenced to planes 1 and 2). To this end, the air sections and supporting beads are deembedded from the cell scattering parameters using the transmission matrix approach presented in [9]. Eventually, from the cell scattering parameters, the complex dielectric spectrum is extracted. Details of this step are given in Section III-D.

B. System Calibration

During the system calibration procedure, we simultaneously characterize the unknown ECU states and calibrate the one-port VNA [see Fig. 2(a)]. We describe the raw reflection coefficient measurement $\widetilde{\Gamma}$ taken by the VNA for a one-port device with reflection coefficient Γ as a bilinear transformation

$$\widetilde{\Gamma} = \frac{E_1 \Gamma + E_2}{1 - E_3 \Gamma} \tag{1}$$

and the unknown VNA calibration coefficients to be determined are E_1, E_2, and E_3. In order to find those unknown parameters, we perform raw reflection coefficient $\widetilde{\Gamma}$ measurements of:

1) a set of N transmission lines, each terminated with all of the unknown ECU reflection coefficients Γ_m^{ECU}, for $m = 1, \ldots, M$; and
2) a known highly reflective load.

Regarding the transmission lines, we make the same assumption as in the multiline TRL method [15], i.e., that the propagation constant γ and characteristic impedance Z_0 of the lines are unknown but the same for all the lines, and that the lengths of the lines l_n, for $n = 1, \ldots, N$, where N is the number of lines, are given. Thus, we can write the reflection coefficient of the nth line terminated with the mth ECU state as:

$$\Gamma_{mn} = \Gamma_m^{\mathrm{ECU}} e^{-2\gamma l_n}. \tag{2}$$

while its measurements $\widetilde{\Gamma}_{mn}$ is related to (2) through (1). In our system, we use five transmission lines with lengths ranging from 60 to 500 mm, while the ECU has four states.

As for the highly reflective load, we assume that its reflection coefficient Γ_R is known, and denote its measurement with $\widetilde{\Gamma}_R$. We realize this load as a 60-mm-long short-circuited line section. We assume the short circuit to be ideal while the line section is described in a similar manner as the calibration transmission lines. Thus, $\Gamma_R = -e^{-2\gamma l_r}$, where l_r is the length of the offset section.

The measurements $\widetilde{\Gamma}_{mn}$, for $n = 1, \ldots, N$ and $m = 1, \ldots, M$, and $\widetilde{\Gamma}_R$ form an overdetermined set of equations. We solve this set using a nonlinear least-squares

approach where as the goal function, we use the residual variance

$$
\begin{aligned}
&\sigma^2 \left(E_1, \; E_2, \; E_3, \Gamma_1^{\mathrm{ECU}}, \ldots, \; \Gamma_M^{\mathrm{ECU}}, \gamma \right) \\
&= \frac{1}{P} \left(\left| \widetilde{\Gamma}_R - \frac{-E_1 e^{-2\gamma l_r} + E_2}{1 + E_3 e^{-2\gamma l_r}} \right|^2 \right. \\
&\quad \left. + \sum_{m=1}^{M} \sum_{n=1}^{N} \left| \widetilde{\Gamma}_{mn} - \frac{E_1 \Gamma_m^{\mathrm{ECU}} e^{-2\gamma l_n} + E_2}{1 - E_3 \Gamma_m^{\mathrm{ECU}} e^{-2\gamma l_n}} \right|^2 \right).
\end{aligned} \tag{3}
$$

where $P = M(N-1) - 3$ is the number of degrees of freedom (i.e., the number $MN + 1$ of observations less the number $M + 4$ of estimated parameters). This function is minimized using the Levenberg–Marquardt algorithm as implemented in the MATLAB *lsqnonlin* function. The starting point for the optimization is taken from an approximate solution described in Appendix A. As a result, we obtain the ECU reflection coefficients Γ_m^{ECU} and the calibration coefficients E_1, E_2 and E_3. These coefficients are then used to calculate the corrected reflection coefficient Γ from its raw measurement $\widetilde{\Gamma}$ using the following formula:

$$\Gamma = \frac{\widetilde{\Gamma} - E_2}{E_1 + E_3 \widetilde{\Gamma}}. \tag{4}$$

It is important to note that our new calibration method is not the only one that can be used to calibrate the system. For example, a simple short-open-load (SOL) calibration would be sufficient to calibrate the one-port VNA while the ECU reflection coefficients could be measured by connecting it to the calibrated VNA. However, in such a case, the problem is to establish definitions of SOL calibration standards: for commercially available connector sizes, these definitions are typically obtained by referencing them to a primary multiline TRL calibration [17], [25].

C. Measurement of Cell Scattering-Parameters

Let us consider a DUT which is a measurement cell [see Fig. 2(b)] with a scattering matrix

$$\mathbf{S} = \begin{bmatrix} S_{11} & S_{12} \\ S_{21} & S_{22} \end{bmatrix} \tag{5}$$

that is connected with port 1 to a calibrated one-port VNA and terminated on port 2 by the ECU with the reflection coefficient Γ^{ECU}. We can easily show that the reflection coefficient Γ measured at the DUT port 1 is given by a bilinear transformation

$$\Gamma = \frac{S_{11} - \Delta \cdot \Gamma^{\mathrm{ECU}}}{1 - S_{22} \Gamma^{\mathrm{ECU}}} \tag{6}$$

where Γ^{ECU} is the reflection coefficient presented by the ECU while $\Delta = S_{11} S_{22} - S_{12} S_{21}$ is the determinant of the DUT scattering matrix (5).

In order to determine the three unknown parameters S_{11}, S_{22}, and Δ of the transformation (6), we measure the reflection coefficients Γ_m at the DUT port 1 for M different ECU states with reflection coefficients Γ_m^{ECU}, where $m = 1, \ldots, M$.[1]

---

[1] The minimum number of states necessary to solve the problem is three; our ECU has four states.

TABLE I
EXTRACTION GOAL-FUNCTION DEFINITIONS

Name	T	R_1	TR_1	TR_1R_2
δ_{21}	1	0	1	1
δ_{11}	0	1	1	1
δ_{22}	0	0	0	1

TABLE II
SUMMARY OF SAMPLE PARAMETERS

Sample	Parameters	Thickness [mm]
PTFE		31.0
isopropanol	2-Propanol pure p.-a. 99.7 %	27.1
ethanol	pure p.-a. 96 % (V/V)	24.4
soil #1	$\theta_m = 0.10\,\text{g/g}$, $\sigma_{\text{KCl}} = 0\,\text{S/m}$	37.4
soil #2	$\theta_m = 0.10\,\text{g/g}$, $\sigma_{\text{KCl}} = 0.5\,\text{S/m}$	37.9
soil #3	$\theta_m = 0.10\,\text{g/g}$, $\sigma_{\text{KCl}} = 1.0\,\text{S/m}$	38.1
soil #4	$\theta_m = 0.10\,\text{g/g}$, $\sigma_{\text{KCl}} = 1.5\,\text{S/m}$	38.0
soil #5	$\theta_m = 0.20\,\text{g/g}$, $\sigma_{\text{KCl}} = 1.0\,\text{S/m}$	36.5
soil #6	$\theta_m = 0.25\,\text{g/g}$, $\sigma_{\text{KCl}} = 1.0\,\text{S/m}$	36.0

The resulting stimuli Γ_m^{ECU} and measurements Γ_m form a set of overdetermined equations that can be solved for parameters S_{11}, S_{22}, and Δ. We use here the linear least-squares approach of [21]. To this end, we form matrices

$$\mathbf{X} = \begin{bmatrix} \Gamma_1 & 1 & \Gamma_1\Gamma_1^{\text{ECU}} \\ \vdots & \vdots & \vdots \\ \Gamma_M & 1 & \Gamma_M\Gamma_M^{\text{ECU}} \end{bmatrix}, \quad \mathbf{y} = \begin{bmatrix} \Gamma_1^{\text{ECU}} \\ \vdots \\ \Gamma_M^{\text{ECU}} \end{bmatrix}, \qquad (7)$$

and write the solution as [21]

$$[-\Delta, \ S_{11}, \ S_{22}]^T = (\mathbf{X}^H\mathbf{X})^{-1}\mathbf{X}^H\mathbf{y} \qquad (8)$$

where the superscript H denotes the matrix Hermitian transpose.

Having determined Δ, S_{11} and S_{22} from (8), we still need to resolve the determinant Δ for S_{12} and S_{21}. Since these two scattering parameters appear in Δ as a product, our method cannot capture the difference in S_{12} and S_{21}, and is therefore applicable only to reciprocal DUTs. For such DUTs, we can write the transmission parameters $S_{21} = S_{12} = \pm(S_{11}S_{22} - \Delta)^{1/2}$ where the proper square root needs to be chosen so as to assure physical meaningfulness of the result. An algorithm for such a root choice is given in [26].

D. Dielectric Spectrum Extraction

Once the scattering parameters of the cell are measured, we proceed with the extraction of the MUT dielectric spectrum. In the extraction procedure, we first determine the scattering parameters of the material sample itself by removing the impact of the air sections and POM beads [see Fig. 2(c)]. We use here the transmission matrix approach discussed in [9]. Scattering parameters of the POM beads are separately measured in our system. Having determined the scattering parameters $\widetilde{S}_{11}$, $\widetilde{S}_{22}$, and $\widetilde{S}_{21}$ of the sample itself, we use an iterative nonlinear-least-squares extraction algorithm. We investigate a class of goal functions written as

$$e(\varepsilon_r) = \delta_{21}|\widetilde{S}_{21} - S_{21}(\varepsilon_r)|^2$$
$$+ \delta_{11}|\widetilde{S}_{11} - S_{11}(\varepsilon_r)|^2 + \delta_{22}|\widetilde{S}_{22} - S_{22}(\varepsilon_r)|^2 \quad (9)$$

where $\delta_{ij} = \{0, 1\}$ depending on the goal function (see Table I) while the model is [6]

$$S_{11}(\varepsilon_r) = S_{22}(\varepsilon_r) = \frac{\Gamma_0(1 - z^2)}{1 - z^2\Gamma_0^2} \qquad (10)$$

$$S_{21}(\varepsilon_r) = S_{12}(\varepsilon_r) = \frac{z\left(1 - \Gamma_0^2\right)}{1 - z^2\Gamma_0^2} \qquad (11)$$

with

$$z = e^{-j\omega/c\sqrt{\varepsilon_r}l_s}, \quad \Gamma_0 = \frac{1 - \sqrt{\varepsilon_r}}{1 + \sqrt{\varepsilon_r}} \qquad (12)$$

TABLE III
PARTICLE-SIZE DISTRIBUTION (PSD) OF THE SOIL MATERIAL

Particle sizes (µm)	PSD (%)
0.01-2	17.28
2-20	62.26
20-50	11.75
50-100	4.07
100-250	3.04
250-500	1.29
500-1000	0.31
1000-2000	0

where z is the transmission through the sample that one would measure in a system that is impedance-matched to the MUT, Γ_0 is the reflection coefficient at the sample interface that one would measure for an infinite sample length, l_s is the sample length, ω is the angular frequency, and c is the speed of light in vacuum. We do not use the reverse transmission $\widetilde{S}_{12}$ in the goal function since we assumed the DUT to be reciprocal (see Section III-C) while the model (11) is the same for the forward and reverse transmission. The goal function (9) is minimized using the Levenberg–Marquardt algorithm as implemented in the MATLAB *lsqnonlin* function. For all goal functions listed in Table I, we use the solution from the noniterative Boughriet's algorithm [27] as a starting point.

IV. MATERIALS

In order to verify the performance of our new one-port setup and compare it to our previous two-port system [9], samples of polytetrafluoroethylene (PTFE), ethanol, and isopropanol were measured. Also, samples of silt loam soil of various moisture content and salinity were prepared. Parameters of the tested samples, including their exact thickness, are shown in Table II.

The volume of ethanol and isopropanol samples was adjusted so as to obtain samples with approximately 25 mm thickness. We used a smaller thickness of alcohol samples than for soil and PTFE in order to reduce the attenuation at higher frequencies and therefore obtain higher measurement accuracy. For the soil samples, we used the thickness of approximately 40 mm. The particle-size distribution of the soil, given in Table III, was measured by laser diffractometer Mastersizer 2000 according to the procedure described in [28]. Samples of various moisture content were obtained by adding a predefined amount of KCl solution of electrical conductivity of 1 S/m to air-dry soil material in order to achieve target mass water contents 0.1, 0.2, and 0.25 g/g (on a dry mass basis). Each sample was thoroughly mixed with the liquid in
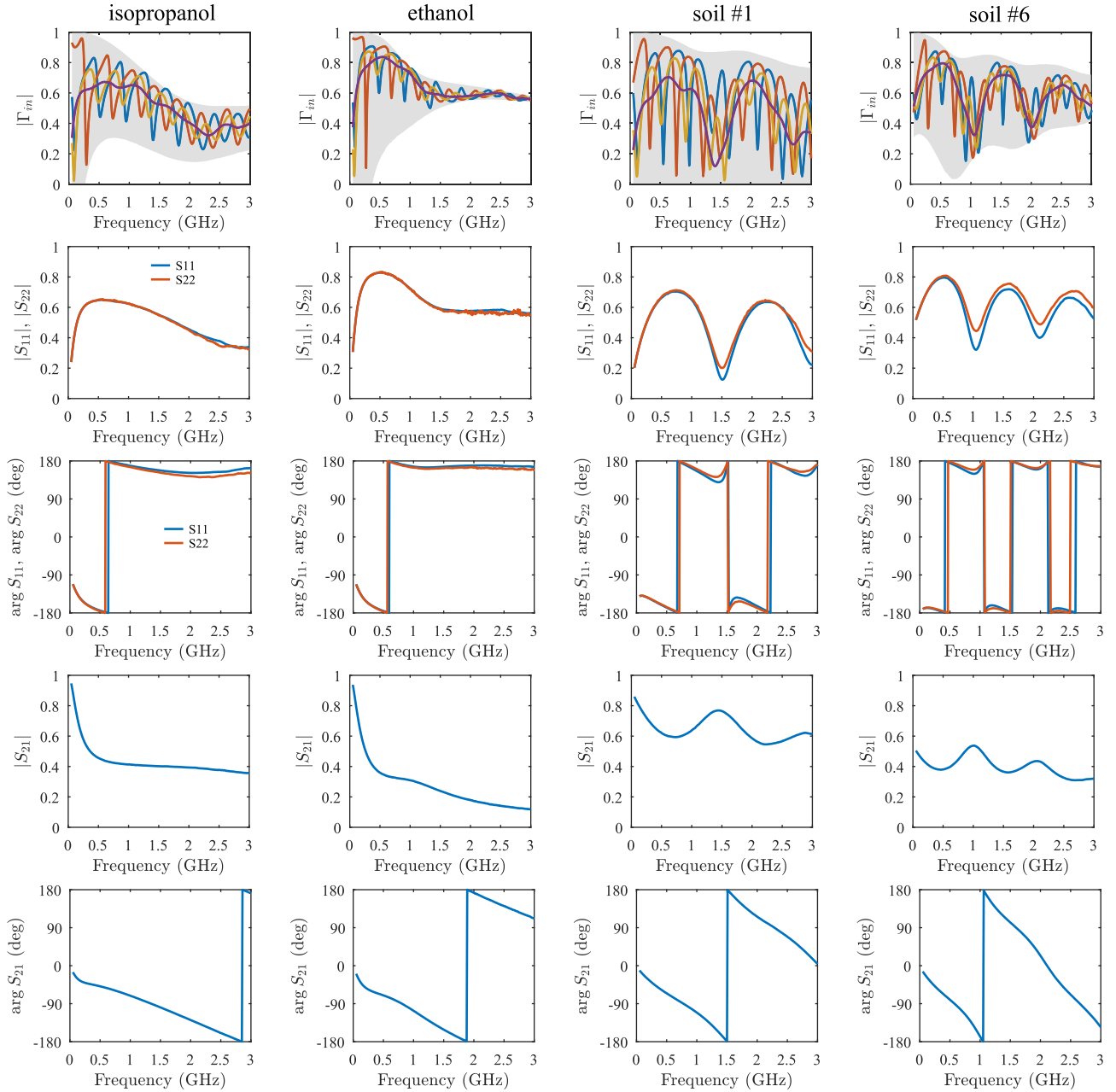
Fig. 3. MUT-sample input reflection coefficients and MUT-sample scattering-parameters obtained in our new one-port system for isopropanol (first column), ethanol (second column), soil #1 (third column), and soil #6 (fourth column). Input reflection-coefficient magnitude (first row) with an interval between the maximum and minimum possible value of $|\Gamma_{\text{in}}|$ indicated with a gray color. Magnitudes of S_{11} and S_{22} (second row). Phases of S_{11} and S_{22} (third row). Magnitude of S_{21} (fourth row). Phase of S_{21} (fifth row).

order to obtain material that is as homogeneous as possible. In order to prepare samples of different salinities, distilled water and three KCl solutions of electrical conductivity 0.5, 1, and 1.5 S/m were added to obtain the same target moisture 0.1 g/g (on a dry mass basis).

V. EXPERIMENTAL RESULTS

We verified the performance of our system in three steps. We first investigated the quality of cell scattering parameter measurements (see Section V-A). After that, we analyzed properties of different extraction algorithms proposed in Subsection III-D (see Section V-B). Then, we compared

dielectric-spectrum extraction accuracy for the new one-port system and the previous two-port system [9] based on measurements of reference materials: PTFE, isopropanol, and ethanol (see Section V-C). Finally, we tested our system in the characterization of soils samples with unknown dielectric properties (see Section V-D).

A. Measurement of Cell Scattering-Parameters

We investigated the scattering parameter measurement performance of our system for ethanol and isopropanol samples and for two selected soil samples (see Table II). We chose soil samples with the best and the worst properties from the

metrological point of view, that is, soil #1 with the lowest and soil #6 with the highest moisture content, respectively.

In Fig. 3, we show the corrected reflection coefficient and scattering parameter measurements obtained in our system. In the first row of plots shown in Fig. 3, we show the magnitude of MUT-sample input reflection-coefficient Γ_{in} [see Fig. 1(c)] for all four ECU states. Underneath these plots, we indicate with a gray color a range covering all possible values of $|\Gamma_{\text{in}}|$ under passive loading Γ_l. This range is calculated from the lower (B.5) and upper (B.4) bound derived in Appendix B. The smaller the possible $|\Gamma_{\text{in}}|$ range the larger needs to be measurement accuracy in order to distinguish changes in Γ_{in} under variation of Γ^{ECU} and, consequently, to determine sample scattering parameters from (8).

We see that for all materials, the measurements are within the indicated bounds which confirm the validity of (B.5) and (B.4). We further note that for all samples, the possible $|\Gamma_{\text{in}}|$ range becomes smaller as the frequency increases due to the increase of MUT loss. We also note that the possible $|\Gamma_{\text{in}}|$ range is smaller for the soil sample with a higher moisture content due to the higher loss.

In the second and third rows of plots shown in Fig. 3, we show the magnitude and phase of S_{11} and S_{22}, respectively. We see that for isopropanol and ethanol both magnitude and phase of S_{11} and S_{22} agree very well, which confirms the validity of our bead and air-section correction algorithm [9]. We further note that at frequencies beyond 2 GHz, the magnitude of S_{22} for ethanol becomes noisy. This effect correlates well with the narrowest $|\Gamma_{\text{in}}|$ range for ethanol at these frequencies, and can be justified with large losses that make the mismatch due to S_{22} and Γ^{ECU} "invisible" at port 1 of the sample. We also observe that for the soil samples, $|S_{22}|$ is slightly larger than $|S_{11}|$ and the discrepancy is larger for the sample with higher moisture content. We think that this effect may be explained with a moisture gradient in the sample, but it needs more investigation.

In the fourth and fifth rows of plots shown in Fig. 3, we depict the magnitude and phase of S_{21}. We do not show corresponding values for S_{12} since all MUTs are reciprocal while our measurement algorithm enforces $S_{21} = S_{12}$ (see Section III-C). We see that for all MUTs, both parameters have smooth frequency dependence which confirms the ability of our measurement algorithm to determine S_{21}, despite high mismatch at the sample input. We see that $|S_{21}|$ at frequencies larger than 2 GHz is the smallest for ethanol, which correlates well with the effect of large losses observed for $|S_{22}|$ of ethanol sample.

In order to better assess the performance of our system, we further defined a figure of merit that is related to the possible $|\Gamma_{\text{in}}|$ ranges shown in the first row of Fig. 3. We observed that the measurement accuracy of our method is limited by small changes of the sample input reflection-coefficient Γ_{in} when the loss increases. In order to accurately measure those small changes, systematic errors introduced by the system must be sufficiently smaller than these changes. We quantify the sample input-reflection-coefficient changes Γ_{in} with a standard deviation σ_{in} over all measured values of Γ_{in} (their
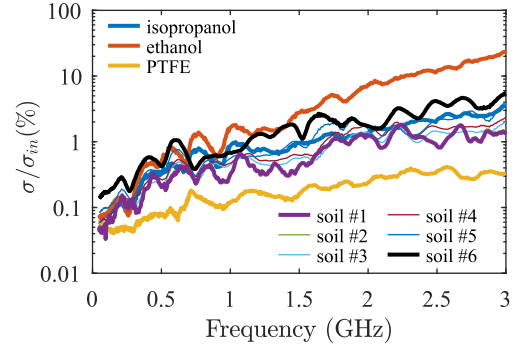

Fig. 4. System relative measurement error (13) for all tested materials.

magnitudes are shown in the first row of the plots shown in Fig. 3). We further approximate the measurement accuracy with the residual standard deviation σ determined from (3) at the solution point. This is a very good approximation of the measurement accuracy, since in our case, the residual variance is calculated over a large sample of measurement errors (five lines with different lengths terminated with four different ECU reflection coefficients). Consequently, our figure of merit becomes

$$\text{FOM} = \frac{\sigma}{\sigma_{\text{in}}} \qquad (13)$$

and informs us how large are the measurement errors relative to the required measurement resolution. Values of this figure of merit are plotted in Fig. 4 for all tested materials. First, we observe that the relative measurement errors increase with frequency since the calibration errors quantified with σ in general, increase with the frequency while σ_{in} decreases with the frequency due to the increase of loss (see the first row of the plots shown in Fig. 3). We further see that the best measurement accuracy is obtained for PTFE which has the smallest losses and the lowest value of dielectric permittivity. The largest relative measurement errors occur for the ethanol sample and are on the order of 20% at 3 GHz. This agrees well with the smallest $|\Gamma_{\text{in}}|$ range and noise in $|S_{22}|$ for ethanol. Based on the values shown in Fig. 3, we may expect the acceptable measurement accuracy for FOM < 10%. This accuracy can be easily adjusted by reducing the sample length.

An *a priori* choice of the sample length can be performed by evaluating (13) for an estimate of the sample dielectric spectrum and then adjusting the sample length such that (13) is below a given threshold in the required frequency range. The value of σ_{in} can then be approximated—as indicated in Appendix B—with (B.11).

B. Extraction Algorithms

In Section III-D, we proposed a class of extraction algorithms (see Table I) based on a nonlinear-least-squares optimization approach. Here, we compare the performance of these algorithms and of the noniterative Boughriet's method [27].

In Fig. 5, we show real ε' and imaginary ε'' parts of dielectric permittivity for isopropanol and ethanol. We observe
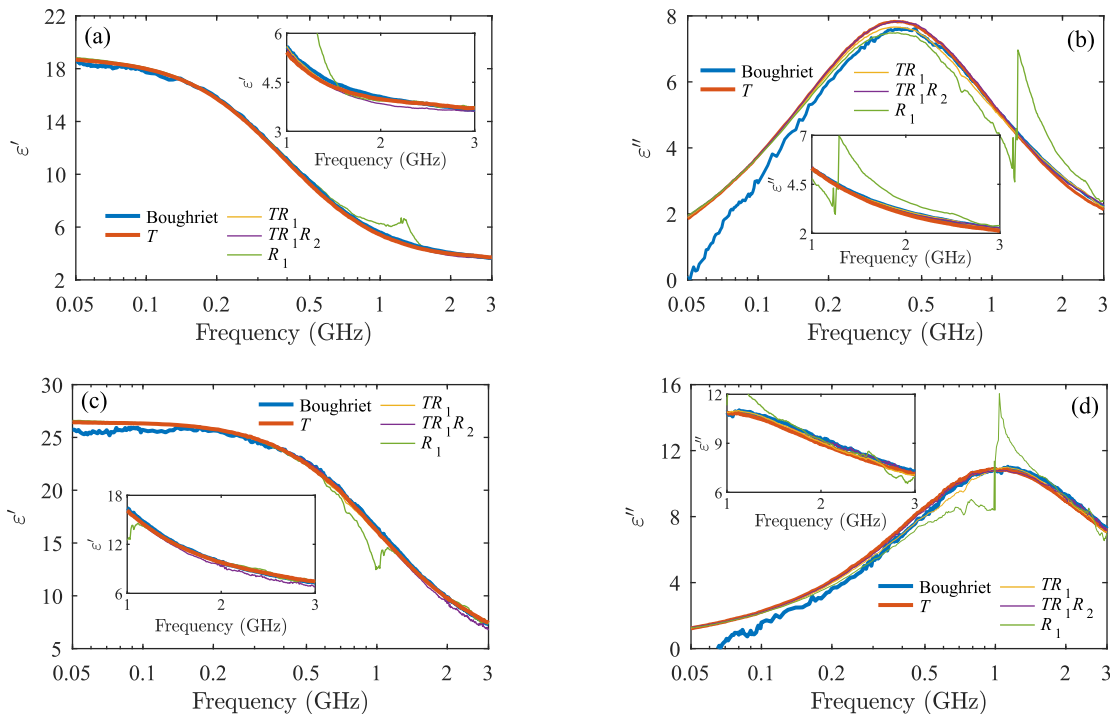
Fig. 5. Isopropanol and ethanol dielectric-spectrum extraction results for different algorithms. (a) and (b) Real ε' and imaginary ε'' parts of isopropanol dielectric permittivity. (c) and (d) Real ε' and imaginary ε'' parts of ethanol dielectric permittivity.
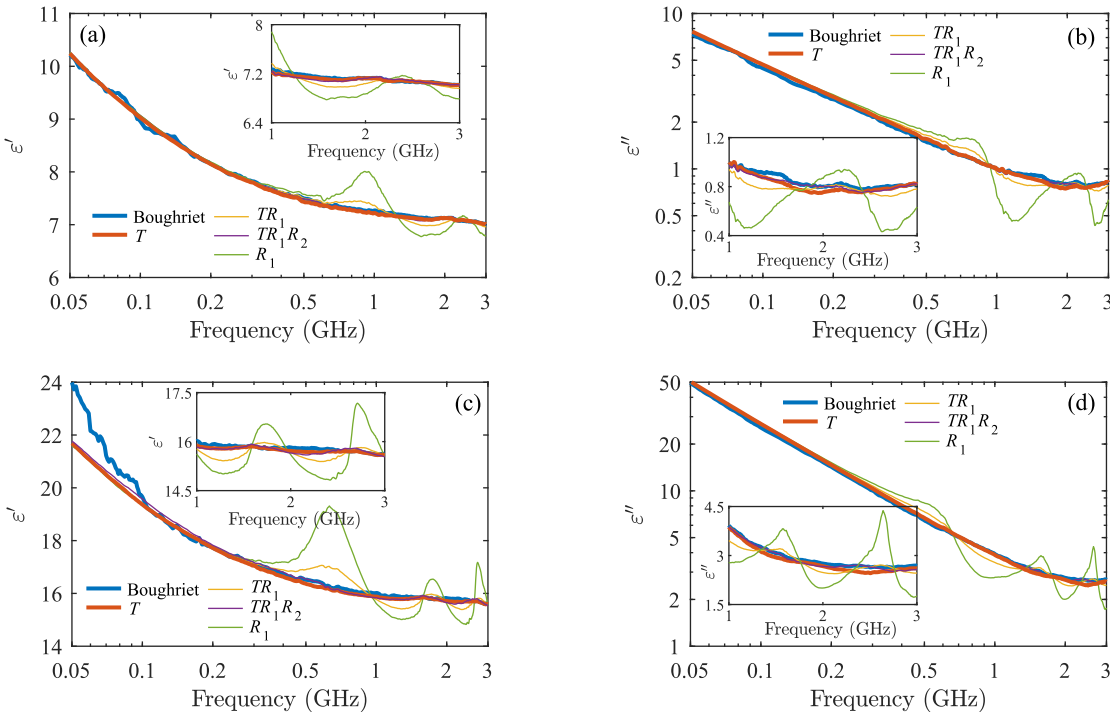

Fig. 6. Soil #1 and soil #6 dielectric-spectrum extraction results for different algorithms. (a) and (b) Real ε' and imaginary ε'' parts of soil #1 dielectric permittivity. (c) and (d) Real ε' and imaginary ε'' parts of soil #6 dielectric permittivity.

that the Boughriet's method (solid thick blue line) works well only over roughly 1 GHz while giving noisy and partially nonphysical results (ethanol ε'' below 70 MHz) below this frequency. We further see that results given by our T algorithm (red solid thick line) which uses only the transmission terms in the goal function (9) agree very well with the Boughriet's

method over 1 GHz while giving much smoother and physical results at frequencies at which the Boughriet's method fails. We also note that the algorithm R_1 (green solid thin line) that accounts only for the reflection coefficient at the sample input clearly fails for all materials giving ripples and spikes. This confirms the well-known fact that the dielectric-spectrum
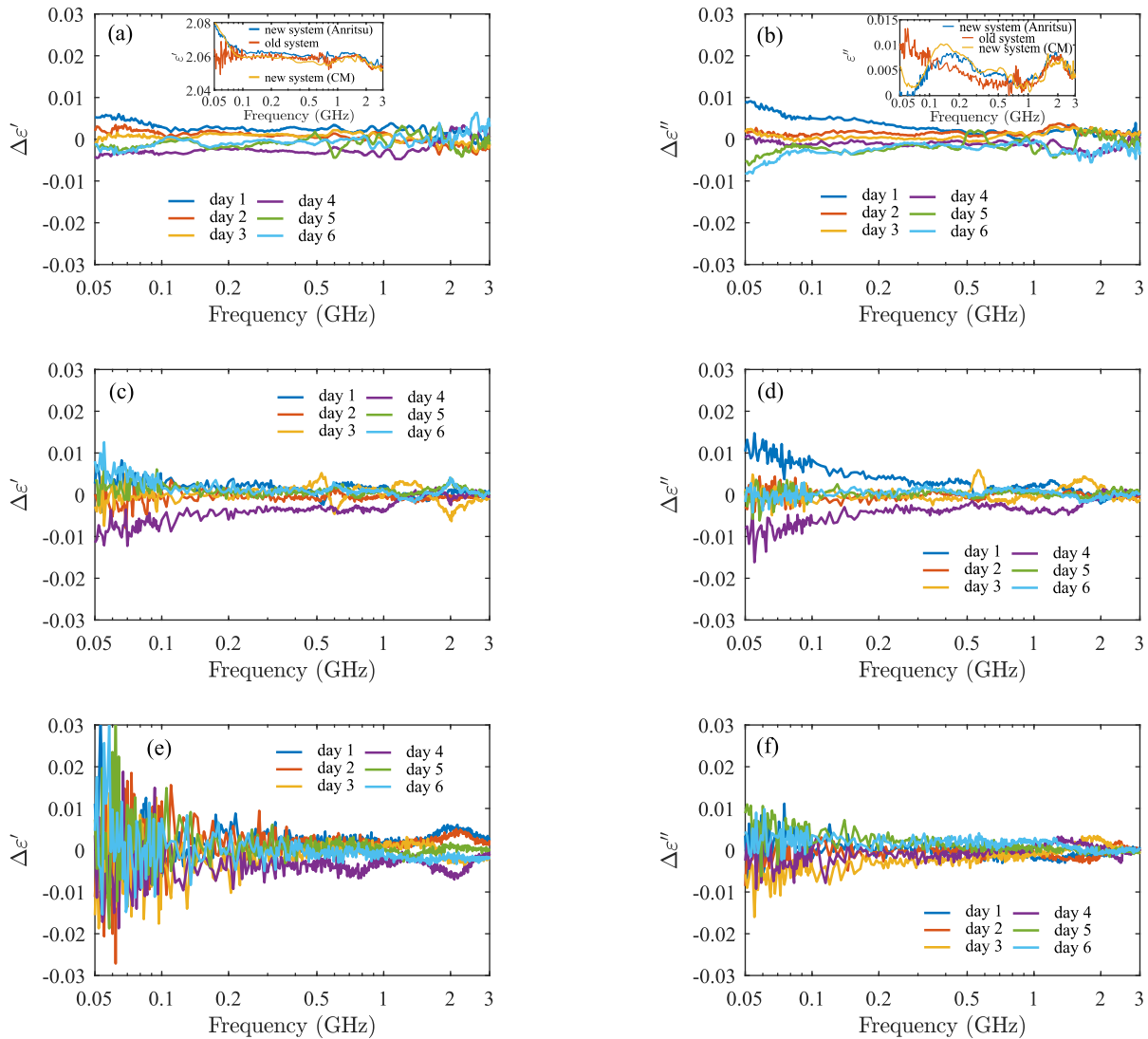
Fig. 7. PTFE-sample dielectric spectrum for six repeated measurements. Differences in (a), (c), (e) real and (b), (d), (f) imaginary parts of the dielectric permittivity with respect to the mean [shown in the insets of (a) (b)] for measurements performed in (a) and, (b) our new one-port-VNA-based system with the Copper Mountain Technologies VNA, (c), (d) our new one-port-VNA-based system with the Anritsu VNA, and (e), (f) in the previous two-port system with the Anritsu VNA [9].

extraction from transmission/reflection measurements is prone to measurement errors in the sample S_{11} and S_{22} [29]. Finally, we see that the algorithms TR_1 and TR_1R_2 which include both transmission and reflection measurements perform better than the R_1 algorithm and comparably with the T algorithm. However, they still give some small ripples (e.g., TR_1 for ethanol ε'' around 0.7 GHz, TR_1R_2 for ethanol ε' above 2 GHz). Thus, we conclude that for isopropanol and ethanol, the T algorithm gives the best results out of all the algorithms under consideration.

In Fig. 6, we present a similar comparison of the dielectric-spectrum extraction results for soil #1 and soil #6 (see Table II). These results confirm that the T algorithm outperforms the Boughriet's method at lower frequencies while yielding similar results at higher frequencies. They also confirm that the T algorithm gives smoother results than the algorithms including reflection measurements. Thus, the T algorithm was chosen in the rest of this paper to extract the dielectric permittivity from the sample scattering parameters.

C. Reference Material Measurements

System performance verification in the measurement of reference materials was conducted in two experiments. First, we compared the new one-port-VNA system and the old two-port-VNA system [9] based on measurements of PTFE. In the second experiment, we focused on the performance of both methods for materials with well-defined properties which are also close to the properties of soil: we chose here isopropanol and ethanol.

In the first experiment, we took six repeated measurements of the same PTFE sample in three different setups: 1) in the new one-port setup with Copper Mountain Technologies R60 VNA; 2) in the new one-port setup with Anritsu Vec-torStar MS4642A as a one-port VNA; and 3) in the previous system [9] with Anritsu VectorStar MS4642A as a two-port VNA. Comparison of measurements in setups 1) and 2) allowed us to evaluate the impact of the VNA itself on the performance of the one-port method while the comparison of measurements in setups 2) and 3) helped us to investigate the
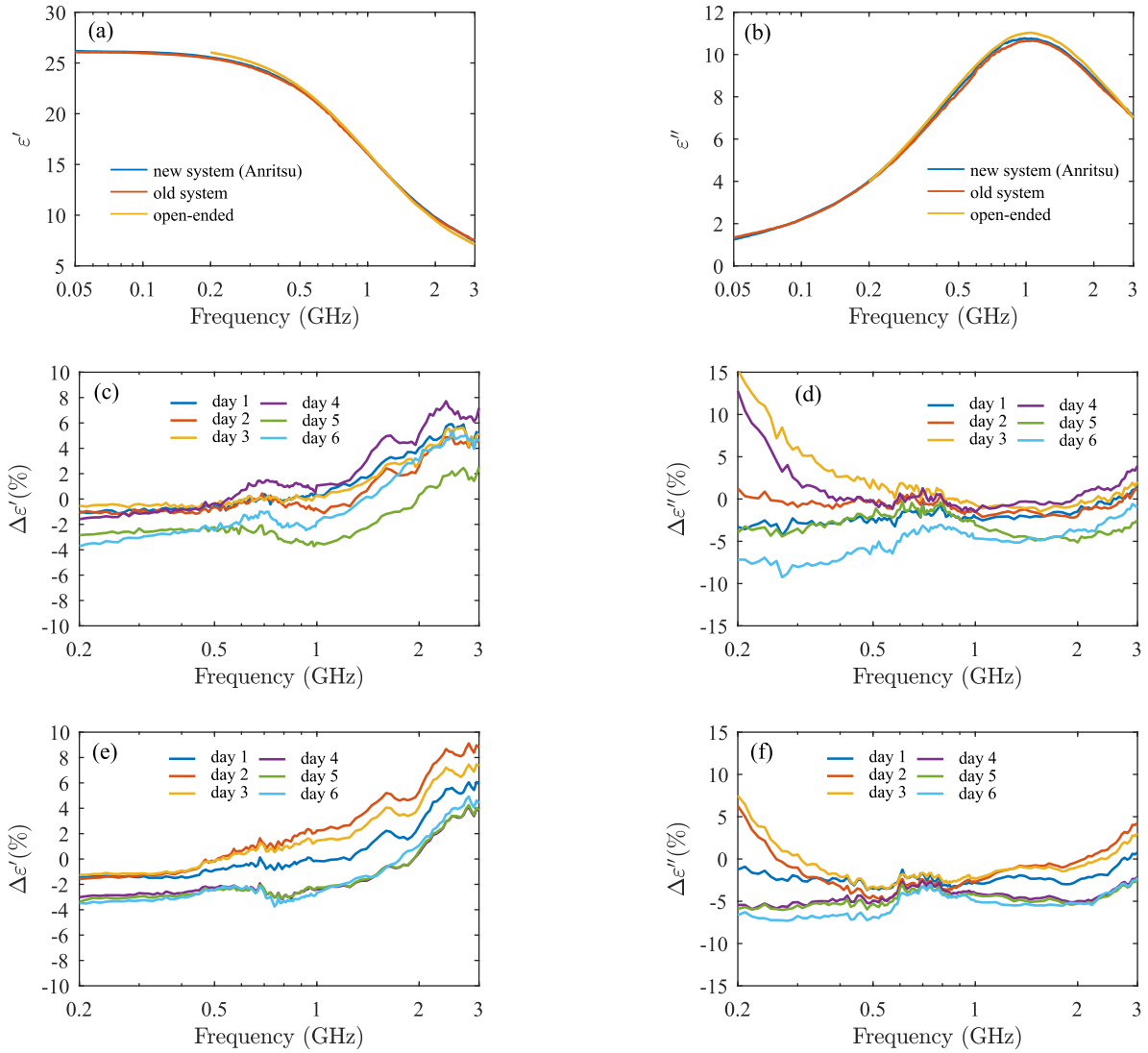
Fig. 8. Ethanol complex dielectric spectrum measured with the new one-port and old two-port systems and the reference open-ended system. (a) and (b) Real and imaginary parts of the mean of repeated measurements (6 for coaxial-cell-based systems and 12 for the open-ended system). (c) and (d) Real and imaginary parts of relative differences between the new one-port-system measurement and the open-ended-system measurement. (e) and (f) Real and imaginary parts of relative differences between the old two-port system measurement and the open-ended-system measurement.

differences between our new one-port and previous two-port measurement method. All measurements were taken at room temperature.

The measurements of the PTFE sample are presented in Fig. 7. Each of the six repeated measurements in a given setup consisted of a single system calibration followed by a measurement of the PTFE sample. For each setup, we calculated the mean of the repeated measurements of the dielectric permittivity as a function of frequency—real and imaginary parts of this mean is shown in the insets of Fig. 7(a) and (b). For each repetition, we then calculated the difference with respect to the mean, and finally illustrated these differences in Fig. 7. In Fig. 7 (a) and (b), we depict the real and imaginary parts of these differences for the results obtained with the new system with Copper Mountain R60 VNA; in Fig. 7(c) and (d), we present the differences for the new system with Anritsu VNA in a one-port-mode; while in Fig. 7 (e) and (f),

we present the differences for the previous two-port Anritsu VNA system [9].

As can be seen, there is much less noise in the spectra measured with the one-port systems. Also, for both parts of the dielectric permittivity, the deviations from the mean are generally within 0.01 for the one-port systems, while for the old one, they can be more than twice larger, especially in the lower part of the frequency range for the real part of dielectric permittivity. We also observe the one-port system with the Copper Mountain VNA yields smoother results than the same system with Anritsu VNA in a one-port mode[2].

---

[2]We found out that this result does not depend on the VNA settings (such as power level or intermediate frequency bandwidth). We believe that it can be attributed to different types of receivers used in both VNAs: Copper Mountain R60 VNA uses mixer based receivers while Anritsu VectorStar MS4642A employs sampler-based receivers.
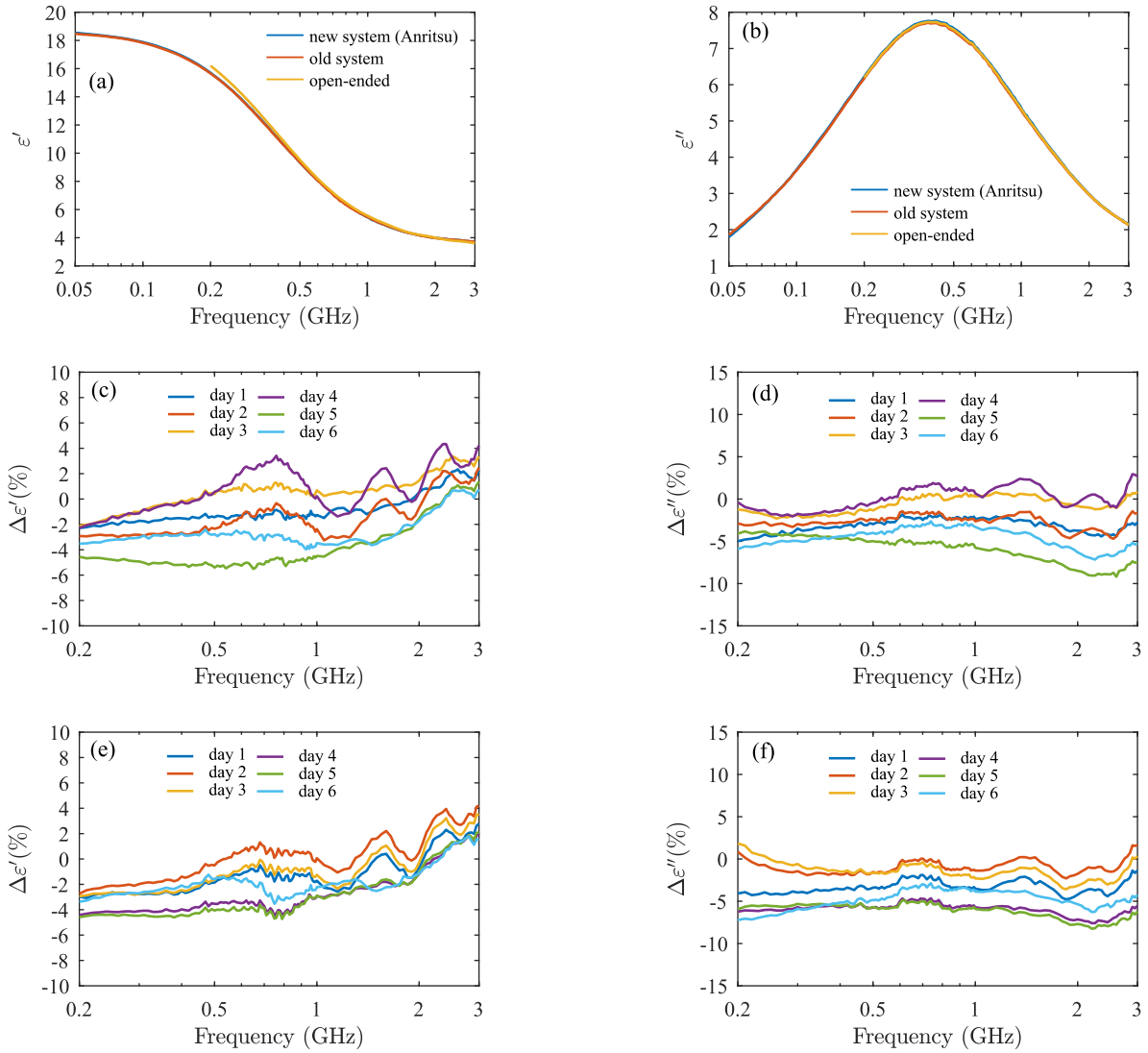
Fig. 9. Isopropanol complex dielectric spectrum measured with the new one-port and old two-port system and the reference open-ended system. (a) and (b) Real and imaginary parts of the mean of repeated measurements (6 for coaxial-cell-based systems and 12 for the open-ended system). (c) and (d) Real and imaginary parts of relative differences between the new one-port-system measurement and the open-ended-system measurement. (e) and (f) Real and imaginary parts of relative differences between the old two-port-system measurement and the open-ended-system measurement.

In the second experiment, we took six repeated measurements of the ethanol and isopropanol sample in setups 2) and 3). For each material, we compared the measurements performed in our systems with reference values obtained with the use of an open-ended probe. We used the DAK-3.5 probe from Schmidt & Partner Engineering AG (SPEAG) connected to R60 VNA from Copper Mountain Technologies. All measurements were taken at room temperature. Measurement results we obtained for ethanol and isopropanol are shown in Figs. 8 and 9, respectively. In Fig. 8(a) and (b), and Fig. 9(a) and (b), the mean values of six measurements obtained with the use of one-port and two-port systems are compared with the reference values from the open-ended probe. The open-ended probe was calibrated with the open-water-short procedure. The reference measurement was performed always before the coaxial-cell-based measurements so as to compensate for the temperature dependence of ethanol and isopropanol dielectric properties.

According to the manufacturer specifications, the lower frequency limit of the SPEAG DAK-3.5 open-ended probe is 200 MHz, thus for the open-ended measurements, we present results in the frequency range from 200 MHz to 3 GHz.

In Fig. 8(c) and (d), and Fig. 9(c) and (d), the relative deviation from the open-ended reference values of the six separate measurements were depicted for the real and imaginary parts, respectively, for the new one-port setup with the Anritsu VNA in the one-port mode. In Fig. 8(e) and (f), and Fig. 9(e) and (f), the deviation of the results from the open-ended values for the old two-port system [9] are presented. First of all, we note that both the one-port and two-port system yield results that agree very well with the reference open-ended measurements. These differences are comparable for both coaxial-cell-based systems and are typically below 9% for ε' and ε'' for both ethanol and isopropanol. Only for two measurements of ethanol, we observe an increase of those
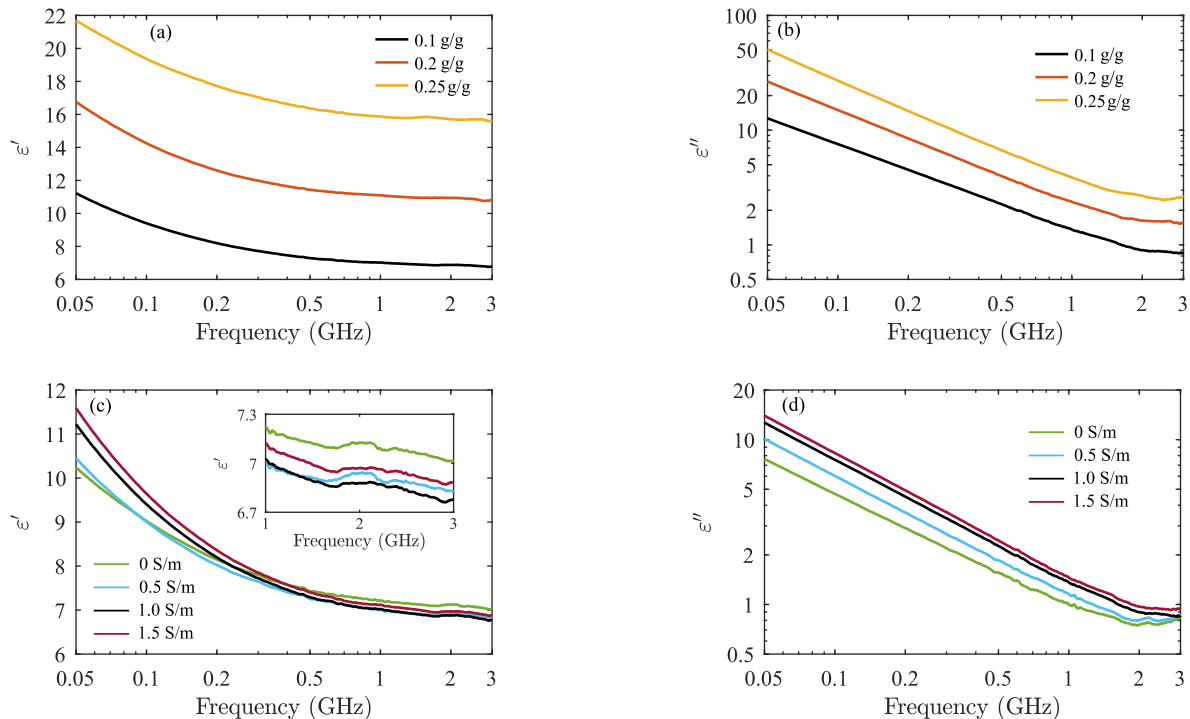
Fig. 10.   Silt loam soil dielectric spectrum for the different salinity level and water content. (a) Real and (b) imaginary parts for electrical conductivity of the moistening KCl solution 1 S/m and mass water contents 0.1, 0.2, and 0.25 g/g. (c) Real and (d) imaginary parts for mass water content 0.1 g/g and electrical conductivity of moistening solutions 0, 0.5, 1.0, and 1.5 S/m (0 refers to distilled water).

differences in ε'' at frequencies below 500 MHz, which can be attributed to a larger temperature drift between the open-ended and coaxial-cell-based measurement.

We further observe that the spread of errors between the coaxial-cell-based systems and the reference open-ended measurement due to the measurement nonrepeatability is below 7% for ε' and ε'' for both ethanol (except for the two outlying measurements below 500 MHz indicated above), and below 5% for ε' and 9% for ε'' for isopropanol, and is comparable for both the one-port and two-port systems. As this spread is also comparable with the systematic errors between the coaxial-cell-based and open-ended measurements, we can approximately state that the coaxial-cell-based systems and the open-ended system yield the same results with the tolerance of the measurement nonrepeatability. Further statistical investigation of those differences would require a full uncertainty analysis of the three systems considered in this experiment and is beyond the scope of this paper.

D. Soil Measurements

In soil measurements, we used the portable one-port R60 VNA from Copper Mountain Technologies which we found to be more accurate than the Anritsu VectorStar MS4642A based on previous PTFE measurements. Complex dielectric permittivity spectra of silt loam samples measured with the one-port system are presented in Fig. 10. The spectra of samples of various moisture content are depicted in Fig. 10(a) and (b), real and imaginary parts, respectively, while the spectra of samples of the same target moisture but various salinity are depicted in Fig. 10(c) and (d).

As expected, moisture content heavily influences both parts of the dielectric permittivity at all frequencies. The impact of sample DC electrical conductivity, which varies with water content and electrical conductivity of moistening solutions, dominates the imaginary part of dielectric permittivity, especially at frequencies below about 1 GHz. However, the salinity of the sample influences also the real part of the dielectric permittivity, which is most evident at frequencies below 0.2 GHz.

The samples whose spectra we show in Fig. 10(c) and (d) were moistened to achieve the same target moisture 0.1 g/g (on a dry mass basis). The differences in high-frequency real dielectric permittivity (shown in the inset) are due to the evaporation and slight density changes during sample preparation and packing in the measurement cell. As one can see, the differences between the fringe spectra do not exceed 5%. We consider that good repeatability of the sample preparation and loading procedure, especially though no special attempt was made to ensure the exact sample bulk density nor prevent slight evaporation. At these frequencies, the influence of salinity on the real part of dielectric permittivity is negligible.

Despite the relatively low moisture content, the impact of the salinity level on the real part of dielectric permittivity is noticeable in Fig. 10(c) in the low-frequency part of the spectrum. Namely, the greater the conductivity of the moistening solution is, the greater the rise in the real part of dielectric permittivity at low frequencies. This is evident even for the sample moistened with distilled water, even though its high-frequency real part of dielectric permittivity is the highest among the four samples. This behavior implies that low-frequency interfacial relaxation phenomena that depend

on sample salinity influence the real part of the dielectric permittivity even at low water content, for which the difference in the imaginary part of dielectric permittivity is not very large.

VI. CONCLUSION

We presented a new one-port-VNA-based system for soil dielectric spectrum characterization which builds on our previously developed two-port-VNA-based system [9]. Performance of this new system was compared with the old two-port-VNA-based setup based on the measurement of reference materials: PTFE, ethanol, and isopropanol. Both systems were found to yield results comparable to within the measurement repeatability. We further used the new system to characterize the dielectric spectrum of silt loam soil samples of various moisture content and salinity. The accuracy of the new system at low frequencies allowed us to capture the impact of the sample salinity on the real part of dielectric permittivity for samples of relatively low moisture content.

The use of the ECU and of the novel vacuum connection system increases the speed and the ease of operation with respect to the two-port VNA setup, and thus increases the measurement robustness. Also, the use of a portable one-port VNA significantly decreases the cost of the system. Our further research will concentrate on the development of a commercial version of the system, which would enable widespread use of soil dielectric testing in the moisture sensors development and in the improvement of GPR and remote sensing techniques.

APPENDIX A
APPROXIMATE SYSTEM CALIBRATION

Approximate system calibration gives an estimate of the unknown parameters E_1, E_2, E_3, $\Gamma_1^{\mathrm{ECU}}, \ldots, \Gamma_M^{\mathrm{ECU}}, \gamma$ that is then used as a starting point for the minimization of the goal function (3). In the approximate calibration, we first fix the propagation constant γ to the value for the air since the EIA 1 5/8″ transmission lines that we use as calibration standards have air as a dielectric. For each ECU state, we then solve a simpler calibration problem which yields an estimate $\hat{\Gamma}_m^{\mathrm{ECU}}$ of the reflection coefficient of the mth ECU state, and estimates $\hat{E}_{1m}$, $\hat{E}_{2m}$, and $\hat{E}_{3m}$ of the VNA calibration coefficients. The estimates $\hat{E}_{1m}$, $\hat{E}_{2m}$, and $\hat{E}_{3m}$ are then averaged over the M results to yield final results.

A calibration problem that we solve for each ECU state can be written based on a bilinear transformation of the reflection coefficient (2) through (1)

$$\widetilde{\Gamma}_{mn} = \frac{E_1 \Gamma_m^{\mathrm{ECU}} \mathrm{e}^{-2\gamma l_n} + E_2}{1 - E_3 \Gamma_m^{\mathrm{ECU}} \mathrm{e}^{-2\gamma l_n}} = \frac{E'_{1m} \mathrm{e}^{-2\gamma l_n} + E_2}{1 - E'_{3m} \mathrm{e}^{-2\gamma l_n}} \quad \text{(A.1)}$$

where the normalized calibration coefficients are defined as

$$E'_{1m} = E_1 \Gamma_m^{\mathrm{ECU}} \quad \text{(A.2)}$$
$$E'_{3m} = E_3 \Gamma_m^{\mathrm{ECU}} \quad \text{(A.3)}$$

For a set of N lines, we obtain a set of overdetermined linear equations from which we determine estimates $\hat{E}'_{1m}$, $\hat{E}_2$, and $\hat{E}'_{3m}$ using the linear least-squares approach. To this end,

we form matrices

$$\mathbf{X} = \begin{bmatrix} \mathrm{e}^{-2\gamma l_1} & 1 & \mathrm{e}^{-2\gamma l_1} \widetilde{\Gamma}_{m1} \\ \vdots & \vdots & \vdots \\ \mathrm{e}^{-2\gamma l_N} & 1 & \mathrm{e}^{-2\gamma l_N} \widetilde{\Gamma}_{mN} \end{bmatrix}, \quad \mathbf{y} = \begin{bmatrix} \widetilde{\Gamma}_{m1} \\ \vdots \\ \widetilde{\Gamma}_{mN} \end{bmatrix}, \quad \text{(A.4)}$$

and write the solution as [21]

$$[\hat{E}'_{1m}, \ \hat{E}_2, \ \hat{E}'_{3m}]^T = (\mathbf{X}^H \mathbf{X})^{-1} \mathbf{X}^H \mathbf{y}.$$

where the superscript H denotes the matrix Hermitian transpose. Using these estimates, we can then write the measurement of the highly reflective standard as

$$\widetilde{\Gamma}_R = \frac{\hat{E}'_{1m} \frac{\Gamma_R}{\Gamma_m^{\mathrm{ECU}}} + \hat{E}_2}{1 - \hat{E}'_{3m} \frac{\Gamma_R}{\Gamma_m^{\mathrm{ECU}}}} \quad \text{(A.5)}$$

which can be easily solved to yield the ECU reflection-coefficient estimate

$$\hat{\Gamma}_m^{\mathrm{ECU}} = \Gamma_R \frac{\hat{E}'_{1m} + \hat{E}'_{3m} \widetilde{\Gamma}_R}{\widetilde{\Gamma}_R - \hat{E}_2}. \quad \text{(A.6)}$$

This result is then used to denormalize the calibration coefficients $\hat{E}'_{1m}$ and $\hat{E}'_{3m}$ through (A.2) and (A.3) to yield estimates $\hat{E}_1$ and $\hat{E}_3$.

APPENDIX B
BOUNDS FOR LOADED-SAMPLE INPUT REFLECTION-COEFFICIENT

Let us consider a two-port network described with scattering matrix (5) and terminated on port 2 with a load with reflection coefficient Γ_l [see Fig. 2(c)]. We can write the input reflection coefficient Γ_{in} as a bilinear transformation [30]

$$\Gamma_{\mathrm{in}} = \frac{S_{11} - \Delta \cdot \Gamma_l}{1 - S_{22} \Gamma_l} \quad \text{(B.1)}$$

where $\Delta = S_{11} S_{22} - S_{21} S_{12}$ is the determinant of matrix (5).

Let us now investigate the bounds on values of Γ_{in} under the assumption that $|\Gamma_l| \leq 1$. This theoretical model describes the situation when the two-port is a material sample with scattering parameters given by (10) and (11) whose input reflection coefficient is measured under varying reflection coefficient of the ECU [see Fig. 2(a)]. In order to solve the above-mentioned problem, we exploit the well-known property of the bilinear transform that it maps generalized circles (line is a special case of a circle) and their interiors into generalized circles and their interiors (or exteriors) [31]. We can show that the circle $|\Gamma_l| = 1$ maps into a circle [31]

$$|\Gamma_{\mathrm{in}} - C| = r \quad \text{(B.2)}$$

where the circle center C and radius r are given by

$$C = \frac{S_{11} - S_{22}^* \cdot \Delta}{1 - |S_{22}|^2}, \quad r = \frac{|S_{12} S_{21}|}{1 - |S_{22}|^2}. \quad \text{(B.3)}$$

We can further easily prove that the interior of the circle $|\Gamma_l| = 1$ maps into the interior of (B.2). Indeed, if the interior of $|\Gamma_l| = 1$ would map into the exterior (B.2), we would have points within $|\Gamma_l| = 1$ that would map into $|\Gamma_{\mathrm{in}}| > 1$. However, this is not possible since a passive two-port network terminated with a passive load is also passive, thus $|\Gamma_{\mathrm{in}}| \leq 1$.

Using (B.2) and (B.3), we can now easily write the upper bound for $|\Gamma_{\text{in}}|$ as

$$\max_{|\Gamma_l| \leq 1} |\Gamma_{\text{in}}| = |C| + r \qquad (B.4)$$

and the lower bound

$$\min_{|\Gamma_l| \leq 1} |\Gamma_{\text{in}}| = \begin{cases} |C| - r & |C| - r \geq 0 \\ 0 & |C| - r < 0 \end{cases} \qquad (B.5)$$

The range of $|\Gamma_{\text{in}}|$ values corresponding to those bounds is illustrated in the first row of plots in Fig. 3 as a gray area.

From the practical point of view, it is of interest to approximate the bounds (B.4) and (B.5) for the cases of high losses, that is when $|z|^2 \ll 1$. Under this assumption, we can write approximately

$$\frac{1}{1 - z^2 \Gamma_0^2} \approx 1 + z^2 \Gamma_0^2 \qquad (B.6)$$

and consequently approximate (10) as

$$\begin{aligned} S_{11} = S_{22} &\approx \Gamma_0(1 - z^2)\left(1 + z^2 \Gamma_0^2\right) \\ &\approx \Gamma_0\left[1 - z^2\left(1 - \Gamma_0^2\right)\right] \end{aligned} \qquad (B.7)$$

and in a similar manner rewrite (11) as

$$S_{21} = S_{12} \approx z\left(1 - \Gamma_0^2\right)\left(1 + z^2 \Gamma_0^2\right) \approx z\left(1 - \Gamma_0^2\right) \quad (B.8)$$

where we neglected higher order terms due to the assumption $|z|^2 \ll 1$. Substituting (B.7) and (B.8) into the circle radius given in (B.3), we obtain—through some tedious but straightforward transformations and after dropping higher order terms—high loss limits of (B.3)

$$r \approx r_* = |z|^2 \frac{\left|1 - \Gamma_0^2\right|^2}{1 - |\Gamma_0|^2}, \qquad (B.9)$$

and

$$C \approx C_* = \Gamma_0 - z^2 \frac{1 - \Gamma_0^2}{1 - |\Gamma_0|^2} j 2 \text{Im}\Gamma_0. \qquad (B.10)$$

Furthermore, taking into account definition (12) of Γ_0 and setting the loss tangent $\tan\delta = -\text{Im}\varepsilon_r/\text{Re}\varepsilon_r$, we can rewrite (B.9) and (B.10) after a series of transformations as

$$r_* = |z|^2 \frac{\left|1 - \Gamma_0^2\right|}{\cos\frac{\delta}{2}}, \qquad (B.11)$$

and

$$C_* = \Gamma_0 - z^2\left(1 - \Gamma_0^2\right) j \tan\frac{\delta}{2}. \qquad (B.12)$$

These results are very important. First of all, we see that at high frequencies for a lossy sample the circle center (B.12) approaches, the reflection coefficient at the sample interface for the case of no reflection from the other sample end. These results clearly confirm the physical intuition: for high losses, we see mainly the first reflection since the reflection from the other sample end is highly attenuated due to $|z|^2 \ll 1$. Furthermore, the spread of the measured input reflection coefficients quantified by (B.11) becomes smaller as the attenuation increases.

We have discussed in Section V-A a figure of merit for our one-port measurement method which is defined as

$$\text{FOM}_1 = \frac{\sigma}{\sigma_{\text{in}}} \qquad (B.13)$$

where σ is the standard deviation of reflection-coefficient measurement errors—estimated by the calibration residual standard deviation (3) determined at the solution—and σ_{in} is the standard deviation of input reflection coefficient Γ_l measured at the sample input under varying reflection-coefficient of the ECU. A justification of this figure of merit is that in order to accurately observe the reflection coefficient changes at the sample input, the measurement errors must be much smaller than those changes. Now, taking into account (B.11), we can approximate $\sigma_{\text{in}} \approx r_*$ which yields

$$\text{FOM}_1 = \sigma \frac{\cos\frac{\delta}{2}}{|z|^2\left|1 - \Gamma_0^2\right|}. \qquad (B.14)$$

We can define a similar figure of merit for a two-port measurement method proposed in [9]. In the case of two-port measurements of a sample with high losses, we need to measure a small transmission approximated by (B.8). Consequently, measurement errors must be much smaller than this transmission. Assuming that the transmission measurement errors in the two-port calibration method [9] are comparable with the reflection coefficient measurement errors in the one-port method (this is a reasonable assumption since we use the same set of standards in both methods), we obtain:

$$\text{FOM}_2 = \frac{\sigma}{|S_{21}|} = \sigma \frac{1}{|z|\left|1 - \Gamma_0^2\right|}. \qquad (B.15)$$

Now, considering that with both methods we measure samples of the same material but with different lengths (hence we have different terms z_1 and z_2 and the same term Γ_0), we may write a ratio of these figures of merit as

$$\frac{\text{FOM}_1}{\text{FOM}_2} = \frac{\cos\frac{\delta}{2}|z_2|\left|1 - \Gamma_0^2\right|}{|z_1|^2\left|1 - \Gamma_0^2\right|} = \frac{|z_2|}{|z_1|^2}\cos\frac{\delta}{2} \leq \frac{|z_2|}{|z_1|^2} \quad (B.16)$$

since $\delta \in \langle 0, \pi/2 \rangle$. This is a very important result. For both measurement methods, their measurement capabilities are limited for highly lossy samples. Result (B.16) shows that in order to obtain a comparable measurement accuracy in both methods, the sample attenuation in the one-port method needs to be half of the sample attenuation in the two-port method. Consequently, the sample length in the one-port method needs to be half of the sample length in the two-port method.

ACKNOWLEDGMENT

REFERENCES

[1] D. A. Robinson *et al.*, "Soil moisture measurement for ecological and hydrological watershed-scale observatories: A review," *Vadose Zone J.*, vol. 7, no. 1, pp. 358–389, 2008.

[2] T. J. Kelleners, D. A. Robinson, P. J. Shouse, J. E. Ayars, and T. H. Skaggs, "Frequency dependence of the complex permittivity and its impact on dielectric sensor calibration in soils," *Soil Sci. Soc. Amer. J.*, vol. 69, no. 1, pp. 67–76, 2005.

[3] Y. Chen and D. Or, "Effects of Maxwell-Wagner polarization on soil complex dielectric permittivity under variable temperature and electrical conductivity," *Water Resour. Res.*, vol. 42, no. 6, p. W06424, Jun. 2006.

[4] M. Loewer, J. Igel, and N. Wagner, "Spectral decomposition of soil electrical and dielectric losses and prediction of *in situ* GPR performance," *IEEE J. Sel. Topics Appl. Earth Observ. Remote Sens.*, vol. 9, no. 1, pp. 212–220, Jan. 2016.

[5] C.-H. Park, A. Behrendt, E. LeDrew, and V. Wulfmeyer, "New approach for calculating the effective dielectric constant of the moist soil for microwaves," *Remote Sens.*, vol. 9, no. 7, p. 732, 2017.

[6] J. Baker-Jarvis, "Transmission/reflection and short-circuit line permittivity measurements," NIST, Gaithersburg, MD, USA, Tech. Note 1341, 1990.

[7] J. Baker-Jarvis *et al.*, "Measuring the permittivity and permeability of lossy materials: Solids, liquids, metals, building materials, and negative-index materials," NIST, Gaithersburg, MD, USA, Tech. Note 1536, 2005.

[8] N. Wagner, M. Schwing, and A. Scheuermann, "Numerical 3-D FEM and experimental analysis of the open-ended coaxial line technique for microwave dielectric spectroscopy on soil," *IEEE Trans. Geosci. Remote Sens.*, vol. 52, no. 2, pp. 880–893, Feb. 2014.

[9] A. Lewandowski, A. Szypłowska, M. Kafarski, A. Wilczek, P. Barmuta, and W. Skierucha, "0.05–3 GHz VNA characterization of soil dielectric properties based on the multiline TRL calibration," *Meas. Sci. Technol.*, vol. 28, no. 2, p. 024007, 2017.

[10] D. Ba and P. Sabouroux, "*EpsiMu*, A toolkit for permittivity and permeability measurement in microwave domain at real time of all materials: Applications to solid and semisolid materials," *Microw. Opt. Technol. Lett.*, vol. 52, no. 12, pp. 2643–2648, 2010.

[11] N. Wagner, K. Emmerich, F. Bonitz, and K. Kupfer, "Experimental investigations on the frequency- and temperature-dependent dielectric material properties of soil," *IEEE Trans. Geosci. Remote Sens.*, vol. 49, no. 7, pp. 2518–2530, Jul. 2011.

[12] K. Lauer, N. Wagner, and P. Felix-Henningsen, "A new technique for measuring broadband dielectric spectra of undisturbed soil samples," *Eur. J. Soil Sci.*, vol. 63, no. 2, pp. 224–238, 2012.

[13] P. P. Bobrov, A. V. Repin, and O. V. Rodionova, "Wideband frequency domain method of soil dielectric property measurements," *IEEE Trans. Geosci. Remote Sens.*, vol. 53, no. 5, pp. 2366–2372, May 2015.

[14] K. Folgerø, "Bilinear calibration of coaxial transmission/reflection cells for permittivity measurement of low-loss liquids," *Meas. Sci. Technol.*, vol. 7, no. 9, p. 1260, 1996.

[15] R. B. Marks, "A multiline method of network analyzer calibration," *IEEE Trans. Microw. Theory Techn.*, vol. 39, no. 7, pp. 1205–1215, Jul. 1991.

[16] W. Wiatr, R. Frender, and M. Zebrowski, "Characterization of microwave absorbing materials using a wideband T/R measurement technique," in *Proc. 17th Int. Conf. Microw., Radar Wireless Commun. (MIKON)*, May 2008, pp. 1–4.

[17] A. Rumiantsev and N. Ridler, "VNA calibration," *IEEE Microw. Mag.*, vol. 9, no. 3, pp. 86–99, Jun. 2008.

[18] W. Kruppa and K. F. Sodomsky, "An explicit solution for the scattering parameters of a linear two-port measured with an imperfect test set (correspondence)," *IEEE Trans. Microw. Theory Techn.*, vol. MTT-19, no. 1, pp. 122–123, Jan. 1971.

[19] R. B. Marks, "Formulations of the basic vector network analyzer error model including switch-terms," in *50th ARFTG Conf. Dig.*, Portland, OR, USA, vol. 32, Dec. 1997, pp. 115–126.

[20] R. F. Bauer and P. Penfield, "De-embedding and unterminating," *IEEE Trans. Microw. Theory Techn.*, vol. MTT-22, no. 3, pp. 282–288, Mar. 1974.

[21] D. Kajfez, "Numerical determination of two-port parameters from measured unrestricted data," *IEEE Trans. Instrum. Meas.*, vol. IM-24, no. 1, pp. 4–11, Mar. 1975.

[22] J. Randa, W. Wiatr, and R. L. Billinger, "Comparison of adapter characterization methods," *IEEE Trans. Microw. Theory Techn.*, vol. 47, no. 12, pp. 2613–2620, Dec. 1999.

[23] W. Wiatr, "A method for embedding network characterization with application to low-loss measurements," *IEEE Trans. Instrum. Meas.*, vol. IM-36, no. 2, pp. 487–490, Jun. 1987.

[24] A. Wilczek, A. Lewandowski, M. Kafarski, A. Szypłowska, J. Szerement, and W. Skierucha, "Złącze linii współosiowych lub falowodowych oraz sposób ich łączenia," Polish Patent Application 422444, Aug. 3, 2017.

[25] M. Zeier, J. Hoffmann, P. Hürlimann, J. Rüfenacht, D. Stalder, and M. Wollensack, "Establishing traceability for the measurement of scattering parameters in coaxial line systems," *Metrologia*, vol. 55, no. 1, p. S23, 2018.

[26] J. Stenarson and K. Yhland, "Automatic root selection for the unknown thru algorithm," in *Proc. 67th ARFTG Conf.*, Jun. 2006, pp. 150–155.

[27] A.-H. Boughriet, C. Legrand, and A. Chapoton, "Noniterative stable transmission/reflection method for low-loss material complex permittivity determination," *IEEE Trans. Microw. Theory Techn.*, vol. 45, no. 1, pp. 52–57, Jan. 1997.

[28] K. Lamorski, A. Bieganowski, M. Z. Ryżak, A. Sochan, C. Sławiński, and W. Stelmach, "Assessment of the usefulness of particle size distribution measured by laser diffraction for soil water retention modelling," *J. Plant Nutrition Soil Sci.*, vol. 117, no. 5, pp. 803–813, 2014.

[29] U. C. Hasar, "A generalized formulation for permittivity extraction of low-to-high-loss materials from transmission measurement," *IEEE Trans. Microw. Theory Techn.*, vol. 58, no. 2, pp. 411–418, Feb. 2010.

[30] D. M. Kerns and R. W. Beatty, *Basic Theory of Waveguide Junctions and Introductory Microwave Network Analysis*. New York, NY, USA: Pergamon, 1967.

[31] H. Schwerdtfeger, *Geometry of Complex Numbers* (Dover Books on Mathematics). New York, NY, USA: Dover, 2012.

Arkadiusz Lewandowski (M'09) received the M.Sc. and Ph.D. degrees (Hons.) in electrical engineering from the Warsaw University of Technology, Warsaw, Poland, in 2001 and 2010, respectively.

In 2002, he joined the Institute of Electronics Systems, Warsaw University of Technology, where he is involved in the research of microwave measurements. From 2002 to 2004, he was with the Telecommunications Research Institute, Warsaw, where he was involved in the development of digital synthesizers of radar signals. From 2004 to 2008, he was a Guest Researcher with the National Institute of Standards and Technology, Boulder, CO, USA. He has authored or co-authored 24 journal papers and over 60 conference papers. His research interests include small- and large-signal microwave measurements, material measurements, and modeling of passive and active microwave devices.

Agnieszka Szypłowska received the M.Sc. and Ph.D. degrees in physics from Maria Curie-Skłodowska University, Lublin, Poland, in 2007 and 2011, respectively.

In 2011, she joined the Institute of Agrophysics, Polish Academy of Sciences, Lublin, where she has been an Assistant Professor since 2013. She is involved in the development of soil moisture and salinity sensors. She has co-authored 18 journal papers, over 20 conference papers, and six Polish patents. Her research interests include the measurements and modeling of soil broadband complex dielectric permittivity spectrum, soil bulk electrical conductivity, and pore-water electrical conductivity.

Andrzej Wilczek received the M.Sc. degree in physics from the Maria Curie-Skłodowska University, Lublin, Poland, in 1998 and the Ph.D. degree in agricultural sciences and the Habilitation degree from the Institute of Agrophysics, Polish Academy of Sciences, Lublin, in 2009 and 2019, respectively.

In 2003, he joined the Institute of Agrophysics, Polish Academy of Sciences, Lublin. He has co-authored more than 50 scientific papers and six Polish patents. His research interests include improvements of time-domain reflectometry methods for soil moisture and salinity measurements as well as electronic devices and sensors for broadband complex dielectric permittivity spectrum measurements.

Marcin Kafarski received the M.Sc. degree in physics from the Maria Curie-Skłodowska University, Lublin, Poland, in 2007 and the Ph.D. degree in electrical engineering from the University of Technology, Lublin, in 2012.

Since 2013, he has been an Assistant Professor with the Institute of Agrophysics, Polish Academy of Sciences, Lublin. His research interests include dielectric sensors for measurement of agricultural materials moisture content, especially soil.

Wojciech Skierucha received the M.S. degree in electronics from the AGH University of Science and Technology, Kraków, Poland, in 1980, and the Ph.D. degree and the Habilitation degree in agricultural sciences from the Institute of Agrophysics, Polish Academy of Sciences, Lublin, Poland, in 1996 and 2006, respectively.

Since 1985, he has been with the Institute of Agrophysics, Polish Academy of Sciences. Since 2014, he has been a Full Professor with the Department of Metrology and Modeling of Agrophysical Properties, Institute of Agrophysics, Polish Academy of Sciences, where he is currently the Head of the Laboratory of Dielectric Spectroscopy. His research interests include TDR and FRD techniques in broadband dielectric spectroscopy, moisture content of soil and materials/products of agricultural origin, agrophysical metrology, and sensors of nonelectrical quantities.

Justyna Szerement received the B.S. and M.S. degrees in chemistry from Maria Curie-Skłodowska University, Lublin, Poland, in 2009 and 2011, respectively, and the Ph.D. degree in agricultural sciences, from the Institute of Agrophysics, Polish Academy of Sciences, Lublin, in 2016.

Since 2017, she has been with the Department of Metrology and Modeling of Agrophysical Processes, Institute of Agrophysics, Polish Academy of Sciences. Her research interests include broadband dielectric spectroscopy, moisture content of soil and agriculture materials, and development and application of sensors.